axioms

IMPACT FACTOR 1.6

Article

Bell Nonlocality and EPR Steering Decay in Dephasing Hyperfine Spins

Kamal Berrada and Smail Bougouffa

Special Issue
Recent Advances in Mathematical Physics with Applications in Quantum Theory

Edited by
Prof. Dr. Oscar Gerardo Loaiza-Brito and Prof. Dr. Hugo García-Compeán

MDPI

https://doi.org/10.3390/axioms14120908

axioms

MDPI

Article

Bell Nonlocality and EPR Steering Decay in Dephasing Hyperfine Spins

Kamal Berrada * and Smail Bougouffa

Department of Physics, College of Science, Imam Mohammad Ibn Saud Islamic University (IMSIU), P.O. Box 90950, Riyadh 11623, Saudi Arabia; sbougouffa@imamu.edu.sa
* Correspondence: kaberrada@imamu.edu.sa

Abstract

This work presents a comprehensive study of quantum correlations and their degradation under environmental dephasing within the atomic hydrogen system. By analyzing the magnetic coupling between the electron and proton spins in the 1*s* hyperfine state, we elucidate how coherent spin interactions generate entangled states and govern their temporal evolution. The investigation focuses on three key measures of quantum correlations—Bell nonlocality, Einstein–Podolsky–Rosen (EPR) steering, and quantum purity—each reflecting a different level within the hierarchy of nonclassical correlations. Analytical formulations and numerical simulations reveal that, in the absence of decay, all quantities remain steady, indicating the preservation of coherence. When dephasing is introduced, each measure decays exponentially toward a stationary lower bound, with Bell nonlocality identified as the most fragile, followed by steering and purity. A three-dimensional analysis of Werner states under dephasing further establishes the critical purity thresholds required for Bell inequality violations. The results highlight the interdependence between magnetic coupling, decoherence, and initial entanglement, providing a unified framework for understanding correlation dynamics in open quantum systems. These findings have direct implications for the development of noise-resilient quantum information protocols and spin-based quantum technologies, where preserving nonlocal correlations is essential for reliable quantum operations.

Keywords: hydrogen atoms; dephasing dynamics; lindblad master equation; bell nonlocality; EPR steering; quantum purity

MSC: 81P40; 81Q93; 81P45; 81S22

Academic Editors: Oscar Gerardo Loaiza-Brito and Hugo García-Compeán

Received: 31 October 2025
Revised: 2 December 2025
Accepted: 9 December 2025
Published: 10 December 2025

Citation: Berrada, K.; Bougouffa, S. Bell Nonlocality and EPR Steering Decay in Dephasing Hyperfine Spins. *Axioms* **2025**, *14*, 908. https://doi.org/10.3390/axioms14120908

1. Introduction

Quantum entanglement has garnered significant attention since the seminal contributions of Einstein and colleagues [1]. This phenomenon involves a unique nonlocal correlation arising from the inseparability of quantum states, serving as a vital resource in advancing key applications within quantum information processing and transmission [2–8]. Specifically, local measurements on separated entangled systems can yield nonlocal correlations [9], which cannot be replicated by local hidden variable models, as evidenced by violations of Bell inequalities [3]. The concept of nonlocality, central to the EPR paradox, challenges quantum mechanics with the notion of "spooky action at a distance" [1]. Schrödinger later described this as quantum steering (or EPR steering), where local measurements can influence a distant quantum subsystem without direct interaction [10].

Quantum steering represents an intermediate form of quantum correlation, positioned between entanglement and Bell nonlocality, and is a key tool for elucidating the EPR paradox in contemporary quantum information theory. Steerable states form a subset of entangled states [11]. Recent theoretical and experimental studies have increasingly focused on quantum steering [12–16], with applications in channel discrimination [17], quantum key distribution [18], and secure teleportation [19]. Furthermore, quantum steering has been interpreted operationally as entanglement distribution involving an untrusted party [20]. Steering inequalities, derived from entropy uncertainty relations, have been developed for both continuous and discrete systems [21–23], and promising criteria for detecting EPR steering have been established to explore its various facets [24,25].

The hydrogen atom, with its fundamentally straightforward structure, has long been a key model in quantum mechanics, providing deep insights into electron–nucleus interactions across various physical, chemical, and biological systems [26–29]. Beyond its central role in quantum theory, the hydrogen atom serves as a critical platform in quantum information science, enabling the study of quantum correlations. The spins of the electron and nucleus in the hydrogen atom create an intuitive framework and a well-defined Hilbert space for exploring bipartite quantum entanglement. This entanglement, measurable through two-qubit concurrence and quantum coherence metrics, is directly tied to fundamental physical constants, including the Planck constant, Boltzmann constant, electron and proton masses, fine-structure constant, Bohr radius, and Bohr magneton. At low temperatures, the hyperfine structure (HFS) states of the hydrogen atom display intrinsic entanglement, which rapidly decreases with rising temperature and vanishes beyond a critical energy threshold of approximately $\tau_c \approx 5.35\,\mu\text{eV}$. This behavior stems from the thermal equilibrium dynamics of the HFS states, where entanglement depends on the interplay between the energy gap and thermal energy [30–32]. Recent investigations into nuclear-polarized phases of hydrogen atoms within solid H_2 films [30,33] have revealed significant deviations from the Boltzmann distribution at low temperatures [30–32], prompting further exploration of quantum effects in these systems. The electron and nuclear spin degrees of freedom in the hydrogen atom offer a versatile platform for studying entanglement with applications in quantum information technologies. Prior studies on electron spin dynamics in two-electron double-quantum-dot systems [34,35] have highlighted their potential as qubits for quantum information processing [4,36,37]. Likewise, nuclear spins, such as those in nitrogen-vacancy centers in diamond, have emerged as promising resources for quantum information applications [38–41]. In contrast to earlier research that focused on electron–proton coordinate entanglement [42] or developed formalisms for HFS entanglement [43], this work reveals a novel finding: an external magnetic field can generate and maintain HFS entanglement at temperatures significantly above the critical threshold τ_c. This magnetically induced entanglement resists the typical thermal decay observed in such systems, opening new possibilities for engineering entanglement in low-temperature settings, including gaseous and solid-state environments.

In open quantum systems, quantum degrees of freedom inevitably interact with surrounding environments, leading to decoherence processes such as dephasing, where phase information is lost without energy exchange, often modeled through the Lindblad master equation [44,45]. This interaction causes the degradation of quantum correlations, including entanglement and coherence, which are essential resources for quantum information tasks [45]. Recent studies on atomic hydrogen have employed open-system frameworks to explore how dephasing affects hyperfine structure dynamics, revealing state-dependent resilience and providing pathways for mitigating noise in quantum technologies [46,47]. These investigations underscore the importance of understanding environmental couplings in realistic settings, from atomic gases to solid-state platforms, to harness quantum effects

for applications like sensing and computation [48]. The novelty of this manuscript lies in its comprehensive examination of the hierarchy of quantum correlations—specifically Bell nonlocality, EPR steering, and quantum purity—within the hyperfine structure of hydrogen atoms subjected to dephasing, extending beyond prior focuses on entanglement and coherence alone [46,49,50]. This allows us to quantify their distinct decay behaviors and identify critical thresholds for nonlocality preservation, providing novel insights into the robustness of higher-order quantum resources in open spin systems. By deriving analytical expressions and conducting numerical simulations, we identify Bell nonlocality as the most fragile correlation, followed by steering and purity, and introduce a three-dimensional analysis of Werner states to pinpoint critical purity thresholds for Bell inequality violations under noise [51]. This unified approach, incorporating magnetic coupling and initial entanglement conditions, not only elucidates the interdependence of decoherence and correlation dynamics but also paves the way for developing robust quantum information protocols in noisy environments, distinguishing it from earlier works on magnetically induced entanglement [50,52].

This manuscript is structured as follows. Section 2 describes the magnetic coupling and quantum states in atomic hydrogen. Section 3 introduces the measures for quantifying quantum correlations, Bell nonlocality, quantum steering, and quantum purity, and discusses their formulations and interpretations. Section 4 presents the numerical results and discussion, analyzing the dynamics of Bell nonlocality, quantum steering, and purity. Finally, Section 5 summarizes the key findings of this study.

2. Magnetic Coupling and Quantum States in Atomic Hydrogen

2.1. Fine Structure of the 1s State

The magnetic interaction in atomic hydrogen stems from the coupling between the fundamental magnetic moments of the electron and proton. For the ground electronic configuration ($1s$), where orbital angular momentum is zero ($\ell = 0$), there exists no orbital magnetic field at the nuclear position. Therefore, the dominant interaction is the direct magnetic coupling between the intrinsic spins of the electron and the proton [29].

This spin–spin coupling manifests as the well-known 21 cm spectral feature (corresponding to 1420 MHz), which has significant importance in both fundamental atomic physics and astronomical observations [53]. From a theoretical perspective, this interaction can be treated using first-order perturbation theory with a Hamiltonian proportional to the dot product of the nuclear and electronic spin vectors:

$$\mathcal{H}_{\mathrm{m}} \propto \vec{\mu}_N \cdot \vec{\mu}_e,$$

where $\vec{\mu}_N$ and $\vec{\mu}_e$ represent the nuclear (proton) and electronic spin operators, respectively. When external magnetic fields are present, this Hamiltonian requires extension to include Zeeman terms [50,53,54].

For two spin-$\frac{1}{2}$ particles (electron and proton), the effective magnetic Hamiltonian can be written using Pauli matrices as

$$\mathcal{H}_{\mathrm{M}} = \alpha\, \vec{\tau}_e \cdot \vec{\tau}_N = \alpha\big(\tau_x^{(e)}\tau_x^{(N)} + \tau_y^{(e)}\tau_y^{(N)} + \tau_z^{(e)}\tau_z^{(N)}\big), \tag{1}$$

where α denotes the magnetic coupling constant ($\alpha \approx 5.88\,\mu\mathrm{eV}/4 = 1.42 \times 10^{-6}\,\mathrm{eV}$, corresponding to the 1420 MHz hyperfine splitting), while $\vec{\tau}_e = (\tau_x^{(e)}, \tau_y^{(e)}, \tau_z^{(e)})$ and $\vec{\tau}_N = (\tau_x^{(N)}, \tau_y^{(N)}, \tau_z^{(N)})$ operate on the electron and nuclear spin spaces, respectively.

The coupling constant α is given explicitly by [53]:

$$\alpha = \frac{\mu_0 g_e g_p e^2 \hbar^2}{12\pi m_e m_p a_0^3}, \tag{2}$$

where μ_0 is the vacuum permeability, a_0 is the Bohr radius, g_e and g_p are the g-factors, and m_e, m_p are the masses of the electron and proton. This formula encapsulates the strength of the magnetic dipole–dipole interaction mediated by the electron probability density at the nucleus.

Each spin-$\frac{1}{2}$ subsystem inhabits a two-dimensional state space spanned by

$$\mathcal{S}_e = \{|+_e\rangle, |-_e\rangle\}, \qquad \mathcal{S}_N = \{|+_N\rangle, |-_N\rangle\}.$$

The composite spin space is therefore

$$\mathcal{S} = \mathcal{S}_e \otimes \mathcal{S}_N = \{|+_e +_N\rangle, |+_e -_N\rangle, |-_e +_N\rangle, |-_e -_N\rangle\}. \tag{3}$$

Diagonalization of $\mathcal{H}_{\mathrm{M}}$ produces an antisymmetric singlet state

$$|\Psi_-\rangle = \tfrac{1}{\sqrt{2}}\big(|+_e -_N\rangle - |-_e +_N\rangle\big), \qquad E_- = -3\alpha, \tag{4}$$

and a symmetric triplet sector

$$|\Phi_+\rangle = |+_e +_N\rangle, \qquad E_+ = \alpha, \tag{5}$$

$$|\Phi_0\rangle = \tfrac{1}{\sqrt{2}}\big(|+_e -_N\rangle + |-_e +_N\rangle\big), \qquad E_0 = \alpha, \tag{6}$$

$$|\Phi_-\rangle = |-_e -_N\rangle, \qquad E_- = \alpha. \tag{7}$$

The magnetic splitting between the singlet and triplet manifolds equals

$$\Delta E = E_\Phi - E_- = 4\alpha \approx 5.88\,\mu\mathrm{eV},$$

where E_Φ indicates the degenerate triplet energy. Without external magnetic fields, the ground state corresponds to the maximally entangled singlet $|\Psi_-\rangle$. Applying a magnetic field removes the degeneracy within the triplet sector, providing external manipulation of the magnetic energy landscape, which is crucial for quantum computing implementations.

2.2. Phase Decoherence in Quantum Evolution

Phase decoherence represents a fundamental noise process in quantum systems where environmental interactions destroy phase relationships between quantum states without altering their occupation probabilities. For the hydrogen atom's magnetic interaction, this type of noise naturally emerges from couplings to external fields or fluctuations that differentially affect the spin components of the electron and proton.

To characterize such decoherence processes quantitatively, we employ the Lindblad framework with local τ_z-type collapse operators, which selectively suppress quantum coherences while preserving energy populations. This methodology offers a mathematically rigorous approach for investigating how quantum entanglement and coherence evolve under phase damping in the two-spin (electron–proton) system.

The time evolution of the density operator $\varrho(t)$ follows the Lindblad equation [44,55–57]:

$$\frac{d\varrho}{dt} = -i[\mathcal{H}_{\mathrm{M}}, \varrho] + \mathcal{L}(\varrho), \tag{8}$$

where $\mathcal{H}_{\mathrm{M}}$ is the magnetic Hamiltonian, $\mathcal{L}(\varrho)$ represents the dissipative superoperator accounting for environmental interactions, and i is the imaginary unit ($i^2 = -1$). For phase damping we employ local dephasing (τ_z-type) Lindblad operators with respective rates κ_e (electron spin dephasing rate) and κ_N (proton spin dephasing rate):

$$M_e = \tau_z^e \otimes \mathbb{I}_N, \qquad M_N = \mathbb{I}_e \otimes \tau_z^N, \tag{9}$$

The dissipator then becomes

$$\mathcal{L}(\varrho) = \kappa_e(M_e \varrho M_e - \varrho) + \kappa_N(M_N \varrho M_N - \varrho), \tag{10}$$

which simplifies due to the property $M_e^2 = M_N^2 = \mathbb{I}$, characteristic of Pauli operators.

We define the coherent coupling frequency $\Omega \equiv \alpha/\hbar$, so that the coherent part of the dynamics is governed by the energy scale $\hbar\Omega = \alpha$. In the standard product basis $\mathcal{S} = \{|1\rangle = |+_e +_N\rangle, |2\rangle = |+_e -_N\rangle, |3\rangle = |-_e +_N\rangle, |4\rangle = |-_e -_N\rangle\}$, the equations of motion for the density matrix components $\varrho_{mn}(t)$ under phase damping read as follows:

Population Dynamics:

$$\frac{d\varrho_{11}}{dt} = 0, \tag{11}$$

$$\frac{d\varrho_{22}}{dt} = -2i\Omega(\varrho_{32} - \varrho_{23}), \tag{12}$$

$$\frac{d\varrho_{33}}{dt} = -2i\Omega(\varrho_{23} - \varrho_{32}), \tag{13}$$

$$\frac{d\varrho_{44}}{dt} = 0. \tag{14}$$

Coherence Evolution:

$$\frac{d\varrho_{12}}{dt} = -2i\Omega(\varrho_{12} - \varrho_{13}) - 2\kappa_N\varrho_{12}, \tag{15}$$

$$\frac{d\varrho_{13}}{dt} = -2i\Omega(\varrho_{13} - \varrho_{12}) - 2\kappa_e\varrho_{13}, \tag{16}$$

$$\frac{d\varrho_{14}}{dt} = -2(\kappa_e + \kappa_N)\varrho_{14}, \tag{17}$$

$$\frac{d\varrho_{23}}{dt} = -2i\Omega(\varrho_{33} - \varrho_{22}) - 2(\kappa_e + \kappa_N)\varrho_{23}, \tag{18}$$

$$\frac{d\varrho_{24}}{dt} = -2i\Omega(\varrho_{34} - \varrho_{22}) - 2\kappa_e\varrho_{24}, \tag{19}$$

$$\frac{d\varrho_{34}}{dt} = -2i\Omega(\varrho_{24} - \varrho_{34}) - 2\kappa_N\varrho_{34}, \tag{20}$$

with $\varrho_{mn}^* = \varrho_{nm}$. These equations explicitly demonstrate the hallmark of pure phase damping: population conservation and exponential decay of off-diagonal coherence terms. Notably, the coupling between ϱ_{22}, ϱ_{33}, and ϱ_{23} illustrates how coherence loss directly affects population transfer between entangled spin configurations.

In the subsequent analysis, we examine the temporal behavior of quantum correlations by solving these equations for physically meaningful initial conditions.

2.3. Initial State and Temporal Evolution

To investigate the dynamics of quantum correlations in the hydrogen magnetic system under Markovian open-system evolution, we consider a family of two-spin entangled states known as X-states. These states are not only physically realizable, but also experimentally accessible, making them suitable for quantum information protocols including teleportation, quantum key distribution, and entanglement-based communication [58–60].

The general X-state takes the following form, parameterized by real numbers $b_1, b_2, b_3 \in [-1, 1]$ and exhibiting maximally mixed reduced density matrices ($\varrho_{e(N)} = \mathbb{I}/2$):

$$\varrho(0) = \frac{1}{4}\begin{pmatrix} 1+b_3 & 0 & 0 & b_1-b_2 \\ 0 & 1-b_3 & b_1+b_2 & 0 \\ 0 & b_1+b_2 & 1-b_3 & 0 \\ b_1-b_2 & 0 & 0 & 1+b_3 \end{pmatrix}. \tag{21}$$

This parameterization includes both maximally entangled Bell states ($|b_1| = |b_2| = |b_3| = 1$) and Werner states ($|b_1| = |b_2| = |b_3| = b$) as special cases, allowing a comprehensive exploration of correlation dynamics.

Within the Markovian approximation, described by the Lindblad master equation, the time-dependent state $\varrho(t)$ maintains the X-structure:

$$\varrho(t) = \begin{pmatrix} \varrho_{11}(t) & 0 & 0 & \varrho_{14}(t) \\ 0 & \varrho_{22}(t) & \varrho_{23}(t) & 0 \\ 0 & \varrho_{32}(t) & \varrho_{33}(t) & 0 \\ \varrho_{41}(t) & 0 & 0 & \varrho_{44}(t) \end{pmatrix}, \tag{22}$$

as confirmed by Equations (11) and (15). This structural preservation is particularly beneficial for analytical studies of entanglement evolution and quantum discord, especially when considering spin-selective decoherence pathways typical of atomic systems.

For transparency and thoroughness, we provide the complete analytical solutions for the time-dependent density matrix elements corresponding to several representative and physically pertinent initial states (Appendix A).

Nonvanishing elements:

$$\varrho_{11}(t) = \varrho_{44}(t) = \tfrac{1}{4}(1+b_3), \tag{23}$$

$$\varrho_{22}(t) = \varrho_{33}(t) = \tfrac{1}{4}(1-b_3), \tag{24}$$

$$\varrho_{14}(t) = \tfrac{1}{4}(b_1-b_2)e^{-2\kappa t}, \tag{25}$$

$$\varrho_{23}(t) = \tfrac{1}{4}(b_1+b_2)e^{-2\kappa t}. \tag{26}$$

Vanishing elements:

$$\varrho_{12}(t) = \varrho_{13}(t) = \varrho_{24}(t) = \varrho_{31}(t) = \varrho_{34}(t) = 0, \tag{27}$$

with $\varrho_{mn} = \varrho_{nm}^*$, where $\kappa = \kappa_e + \kappa_N$.

Having established the dynamical evolution under phase damping, we proceed to examine trace-distance-based classical and quantum correlations, followed by a detailed comparison.

3. Quantifying Nonlocality, Steering, and Purity

This section introduces three complementary measures for characterizing quantum correlations in bipartite systems: Bell nonlocality, quantum steering, and quantum purity. Each measure captures distinct aspects of quantum behavior and operates within a well-defined resource-theoretic framework. We present their mathematical formulations and discuss their physical interpretations in the context of two-qubit systems.

3.1. Bell Nonlocality: Beyond Local Hidden Variable Theories

Bell nonlocality provides the most stringent test of quantum correlations by examining whether observed statistics can be reproduced by any local hidden variable (LHV) theory. The violation of Bell inequalities certifies that nature cannot be described by local realistic models. For two-qubit systems, the Clauser–Horne–Shimony–Holt (CHSH) inequality serves as the canonical test.

The maximum Bell-CHSH parameter for a quantum state is given by [9,61–64]

$$B_{\max} = 2\max\{B_1, B_2\}, \tag{28}$$

where

$$B_1 = \sqrt{\lambda_1 + \lambda_2}, \tag{29}$$

$$B_2 = \sqrt{\lambda_1 + \lambda_3}, \tag{30}$$

and the correlation parameters λ_1, λ_2, and λ_3 are determined by the density matrix elements:

$$\lambda_1 = 4(|\varrho_{14}| + |\varrho_{23}|)^2, \quad \lambda_2 = 4(|\varrho_{14}| - |\varrho_{23}|)^2, \quad \lambda_3 = (\varrho_{11} - \varrho_{22} - \varrho_{33} + \varrho_{44})^2. \tag{31}$$

A violation of the classical bound ($B_{\max} > 2$) unequivocally demonstrates Bell nonlocality. Importantly, this represents a stronger condition than basic entanglement—there exist mixed states that are entangled yet do not violate any Bell inequality. This distinction is particularly evident for X-states, whose analytical tractability makes them ideal for studying the hierarchy of quantum correlations.

3.2. Quantum Steering: Asymmetrical Nonlocal Correlations

Quantum steering represents an intermediate form of nonlocality that is stronger than entanglement but weaker than Bell nonlocality. It captures the ability of one party to remotely affect another's state through local measurements, in a way that cannot be explained by local hidden state (LHS) models. We employ an entropic steering criterion based on conditional uncertainty relations.

Building on the foundational work of Walborn et al. [1–3], the steering condition for continuous variables requires

$$h(x^B|x^A) \geq \int d\lambda\, p(\lambda)\, h_q(x^B|\lambda), \tag{32}$$

where $h_q(x^B|\lambda)$ denotes the continuous Shannon entropy of the conditional probability distribution $p(x^B|\lambda)$. Here, the continuous Shannon entropy is defined as

$$h(x^b|\lambda) = -\int p(x^b|\lambda)\, \log p(x^b|\lambda)\, dx^b, \tag{33}$$

which quantifies the degree of uncertainty in the measurement outcomes of the observable x^b, conditioned on the hidden variable λ. In contrast, the von Neumann entropy,

$$S(\varrho) = -\mathrm{Tr}(\varrho \log \varrho), \tag{34}$$

characterizes the intrinsic mixedness of the quantum state itself, rather than the uncertainty associated with measurement outcomes.

For position-momentum measurements, the LHS model constraint becomes

$$h(x^B|x^A) + h(k^B|k^A) \geq \log(\pi e). \tag{35}$$

Extending this to discrete systems, we obtain the steering inequality for complementary observables:

$$H(R^B|R^A) + H(S^B|S^A) \geq \log(\Omega^B), \tag{36}$$

where $\Omega^B = \min_{i,j}\left(1/|\langle R_i|S_j\rangle|^2\right)$, with $\{|R_i\rangle\}$ and $\{|S_i\rangle\}$ representing eigenbases in an d-dimensional Hilbert space.

For two-qubit systems with Pauli measurements, this simplifies to

$$H(\sigma_x^B|\sigma_x^A) + H(\sigma_y^B|\sigma_y^A) + H(\sigma_z^B|\sigma_z^A) \geq 2. \tag{37}$$

Violation of this bound certifies quantum steering.

For X-states on the computational basis, after appropriate local unitary transformations and Bloch decomposition with vectors $\vec{r} = (0,0,r)$ and $\vec{s} = (0,0,s)$, the steering criterion becomes

$$\begin{aligned}
&\sum_{i=1,2}[(1+c_i)\log(1+c_i) + (1-c_i)\log(1-c_i)] - (1+r)\log(1+r) - (1-r)\log(1-r) \\
&+ \frac{1}{2}(1+c_3+r+s)\log(1+c_3+r+s) + \frac{1}{2}(1+c_3-r-s)\log(1+c_3-r-s) \\
&+ \frac{1}{2}(1-c_3-r+s)\log(1-c_3-r+s) + \frac{1}{2}(1-c_3+r-s)\log(1-c_3+r-s) \leq 2,
\end{aligned} \tag{38}$$

where the correlation parameters are

$$c_1 = 2(\varrho_{23} + \varrho_{14}), \tag{39}$$

$$c_2 = 2(\varrho_{23} - \varrho_{14}), \tag{40}$$

$$c_3 = \varrho_{11} - \varrho_{22} - \varrho_{33} + \varrho_{44}, \tag{41}$$

$$r = \varrho_{11} + \varrho_{22} - \varrho_{33} - \varrho_{44}, \tag{42}$$

$$s = \varrho_{11} - \varrho_{22} + \varrho_{33} - \varrho_{44}. \tag{43}$$

The coefficients c_1 and c_2 encode the coherence properties governing σ_x and σ_y measurements, while r, s, and c_3 characterize population imbalances relevant for σ_z correlations. The left-hand side represents the total conditional uncertainty, with values below 2 indicating that Alice's measurements can reduce Bob's uncertainty beyond classical limits, thus demonstrating steering.

In our electron–proton system, steering analysis reveals directional aspects of quantum correlations that entanglement measures alone cannot capture. From an experimental perspective, steering correlations could be probed through spin-resolved detection techniques, such as optical pumping combined with polarization measurements or atomic-beam spectroscopy.

3.3. Quantum Purity: Quantifying State Mixedness

Quantum purity is a fundamental indicator of the coherence and mixedness of a quantum state, offering key insights into the mechanisms of decoherence. For a density matrix ϱ, purity is defined as [65,66]

$$\mathcal{P}(\varrho) = \mathrm{Tr}(\varrho^2), \tag{44}$$

with bounds $1/d \leq \mathcal{P}(\varrho) \leq 1$, where d denotes the dimension of the Hilbert space. In the case of two-qubit systems ($d = 4$), the purity ranges from $1/4$ for a maximally mixed state to 1 for a pure state.

Physically, purity quantifies the degree of quantum coherence present in a system. States with high purity ($\mathcal{P} \approx 1$) retain strong quantum coherence, a prerequisite for reliable

quantum information processing, whereas low-purity states signify significant decoherence or classical mixing [45,67]. The time evolution of purity under environmental coupling provides a powerful diagnostic of quantum-to-classical transitions. Experimental approaches for assessing purity without resorting to full quantum state tomography include (i) simultaneous measurements on multiple identical copies of a state, (ii) statistical estimation through random measurement bases, and (iii) direct purity determination from quantum interference visibility. In atomic systems such as hydrogen, purity dynamics may be inferred from spectroscopic observations of the 21 cm hyperfine transition [68]. From a quantum information perspective, purity serves multiple essential functions [69]: it acts as a diagnostic of coherence times and qubit quality, a performance metric in quantum error correction and benchmarking protocols, and a probe of dominant noise mechanisms through its temporal behavior. In the electron–proton two-qubit system, the evolution of purity under dephasing provides deep insight into the persistence of quantum coherence in naturally occurring atomic systems. This analysis carries implications for quantum memory applications and for probing the foundations of quantum mechanics in astrophysical contexts. Notably, the X-state structure, which remains invariant under phase damping, allows an analytical description of purity evolution, making such states exemplary for exploring the interplay between coherence, entanglement, and mixedness in open quantum systems.

4. Numerical Results and Discussion

In this section, we investigate the time-dependent behavior of three fundamental quantum properties—Bell nonlocality, steering, and purity—in the hyperfine states of the hydrogen atom. By employing the Lindblad formalism to model pure dephasing and other decoherence channels, we analyze how these distinct forms of quantum correlation evolve under environmental influences. Bell nonlocality provides the most stringent test of quantum correlations by probing violations of local hidden variable theories, while steering captures asymmetric control capabilities between the electron and nuclear spins, and purity quantifies the degree of state mixedness and coherence loss. Together, these metrics offer complementary perspectives: Bell nonlocality reveals the strongest form of quantum correlations, steering demonstrates directional quantum influence, and purity monitors global coherence preservation. The following results highlight the intricate interplay between coherent dynamics driven by the hyperfine interaction and dissipative effects arising from external noise, revealing the hierarchical relationship and differential robustness of these quantum properties under decoherence.

4.1. Analysis of Bell Nonlocality Dynamics Under Dephasing

This section presents a detailed analysis of the temporal evolution of Bell nonlocality for two distinct initial states under varying dephasing strengths. Figure 1 illustrates the time dependence of the Bell parameter as a function of the scaled time t (in units of $1/\Omega$) for different values of the decoherence rate κ. In the subfigure (a), the dynamical behavior of the Bell parameter for this configuration reveals several essential features; in the coherent regime ($\kappa = 0$), blue solid line), the Bell parameter remains constant throughout the evolution, indicating a steady and sustained violation of the Bell inequality. This stationary behavior confirms that, in the ideal coherent regime, Bell nonlocality persists indefinitely without degradation. Under weak dephasing ($\kappa = 0.02\ \Omega$, red dashed line), the Bell parameter exhibits a slow exponential decrease with time, characteristic of Markovian dephasing. This gradual suppression of nonlocality reflects the sensitivity of the system to even minimal environmental interactions. For moderate dephasing ($\kappa = 0.05\ \Omega$, black dash-dotted line), the decay becomes more pronounced, leading to a complete transition from nonlocal to local behavior within a finite timescale. The accelerated loss of nonlocal

correlations highlights the fragility of Bell nonlocality compared with other forms of quantum correlations. In the strong dephasing regime ($\kappa = 0.5\ \Omega$, green dotted line), the Bell parameter rapidly decreases to a minimal steady value, referred to as the lower bound. This behavior signifies the near-complete destruction of nonlocal correlations on timescales much shorter than the coherent period, reminiscent of a Zeno-like suppression induced by strong environmental coupling. As shown in Figure 1, the classical bound for Bell nonlocality is represented by the solid black line at $B_{max} = 2$, with values above this threshold signifying genuine quantum nonlocal correlations. The second configuration, subfigure (b), provides insights into the state-dependent characteristics of Bell nonlocality evolution. The system initially exhibits a higher Bell parameter, indicating stronger nonlocal correlations than in the previous case. In the coherent limit ($\kappa = 0$), the Bell parameter again remains constant, confirming the absence of decay behavior in the non-dissipative regime. The upper bound remains constant in this scenario and exceeds the value observed in the previous case. When dephasing is introduced, the decay follows an exponential trend for all values of κ. However, the enhanced initial correlations in this configuration provide slightly greater resilience against weak dephasing ($\kappa = 0.02\ \Omega$), as the Bell parameter maintains nonclassical values for a longer duration. For larger dephasing strengths, the Bell parameter approaches the lower bound, which is larger than that observed in panel (a), although the decay onset is marginally delayed. Moreover, in this configuration, the range of variation for the Bell nonlocality is more constrained, exhibiting reduced amplitude in its dynamical fluctuations compared to the previous case. Indeed, the observed compression in the range of Bell nonlocality variation for initial state (b) compared to state (a) has a direct physical origin in the structure of quantum correlations. The parameters $b_1(0)$, $b_2(0)$, and $b_3(0)$ in the X-state formulation are not independent; they are constrained by the requirement that the density matrix must be physically valid (positive semidefinite with trace one). State (b), defined by $b_1(0) = 1$, $b_2(0) = -0.9$, $b_3(0) = 0.9$, is significantly closer to the boundary of the physical state space than state (a). This proximity to the edge of allowed states imposes a stronger constraint on the dynamics.

The coherent hyperfine interaction, governed by Hamiltonian Equation (1), acts to rotate the state within this constrained space. For a state like (b) that is initially highly correlated and already near the maximum possible nonlocality for its specific correlation configuration, the margin for dynamical variation is reduced. The state is, in a sense, initially precompressed against a physical boundary, limiting the amplitude of its variations in the Bell parameter. In contrast, state (a) resides in a more central region of the state space, allowing for a wider dynamical excursion as its correlations are transformed by the unitary evolution. Therefore, the compressed variation is a direct manifestation of the initial state's position within the physically allowed manifold of quantum states. Notably, the initial state in (a) decays below this classical bound more rapidly under decoherence, whereas the state in (b) exhibits enhanced robustness, maintaining nonlocal correlations for a significantly longer duration.

The overall analysis demonstrates that dephasing universally suppresses Bell nonlocality through exponential decay, with the rate and persistence time determined by both the decoherence strength and the initial state preparation. The hyperfine coupling parameter Ω defines the natural timescale of coherent evolution, while the ratio κ/Ω quantifies the relative efficiency of decoherence-induced localization. These results clearly indicate the fragile nature of Bell nonlocality, as even weak environmental couplings suffice to eliminate Bell violations within a finite time. The observed dependence on the initial state further underscores the importance of optimizing the preparation of entangled states to extend the persistence of nonlocal correlations in realistic, noisy environments. Finally, the hierarchical decay of quantum correlations—with Bell nonlocality typically being the most susceptible

to decoherence—has significant implications for quantum information processing. Protocols that rely on nonlocal resources must therefore incorporate dedicated error-mitigation or dynamical decoupling techniques to preserve these delicate quantum features against environmental noise.

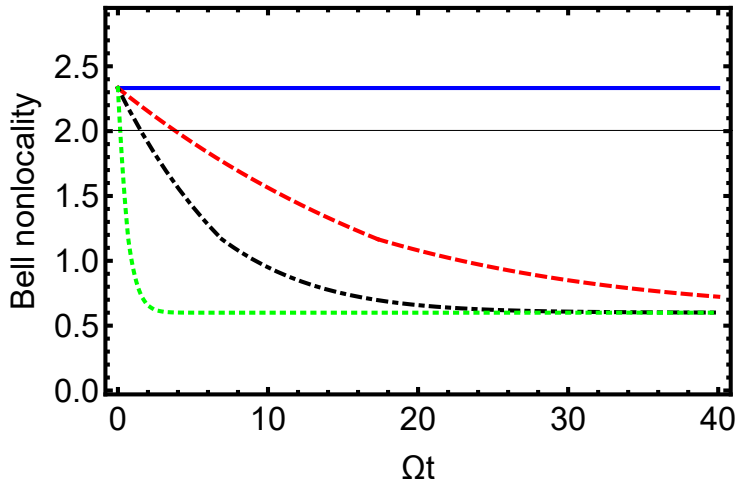

(**a**)

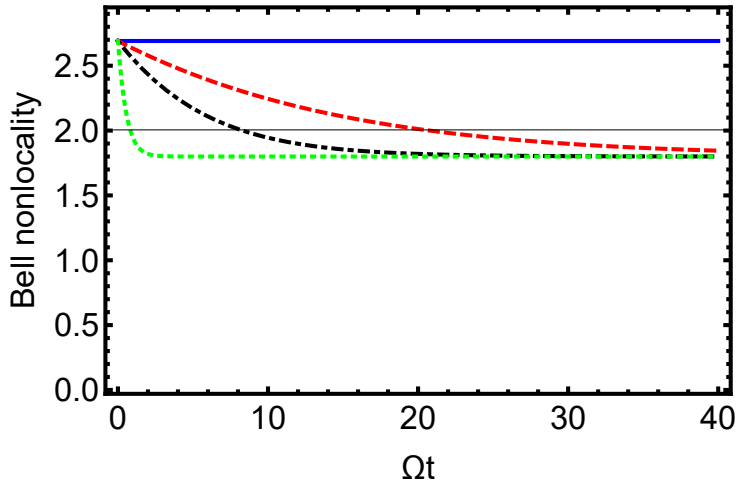

(**b**)

Figure 1. Time evolution of the Bell nonlocality as a function of dimensionless time Ωt for initial conditions $b_1(0) = 1$, $b_2(0) = -0.6$, and $b_3(0) = 0.3$. Subfigures (**a**,**b**) depict the dynamics of Bell nonlocality for different initial states: (**a**) $b_1(0) = 1$, $b_2(0) = -0.6$, $b_3(0) = 0.3$; and (**b**) $b_1(0) = 1$, $b_2(0) = -0.9$, $b_3(0) = 0.9$. The blue line represents $\kappa = 0$, the red dashed line corresponds to $\kappa = 0.02\ \Omega$, the black dash-dotted line indicates $\kappa = 0.05\ \Omega$, and the green dotted line denotes $\kappa = 0.5\ \Omega$, illustrating the effect of increasing decoherence on the quantum steering measure. The solid black line at $B_{\max} = 2$ represents the classical bound.

4.2. Analysis of Quantum Steering Dynamics Under Dephasing

Figure 2 illustrates the temporal evolution of quantum steering, revealing distinct characteristics compared to Bell nonlocality and demonstrating intermediate robustness against dephasing. In subfigure (a), corresponding to initial state $[b_1(0) = 1, b_2(0) = -0.6, b_3(0) = 0.3]$, the coherent regime ($\kappa = 0$) exhibits sustained steady behavior, while weak dephasing ($\kappa = 0.02\ \Omega$) shows only moderate decay of steering capability. Subfigure (b), representing the more strongly correlated initial state $[b_1(0) = 1, b_2(0) = -0.9, b_3(0) = 0.9]$, demonstrates enhanced persistence of steering under identical dephasing conditions, particularly evident in the $\kappa = 0.02\ \Omega$ and $\kappa = 0.05\ \Omega$ cases where steering values remain

significantly above the classical bound for extended durations. As dephasing intensifies ($\kappa = 0.05\ \Omega$), both panels show gradual decay while maintaining steering longer than Bell nonlocality, confirming its intermediate position in the quantum correlation hierarchy. In the strong dephasing limit ($\kappa = 0.5\ \Omega$), steering rapidly diminishes in both configurations, though the decay occurs more progressively than Bell nonlocality's abrupt disappearance, particularly noticeable in panel (b) where residual steering persists slightly longer due to the initial state's stronger quantum correlations.

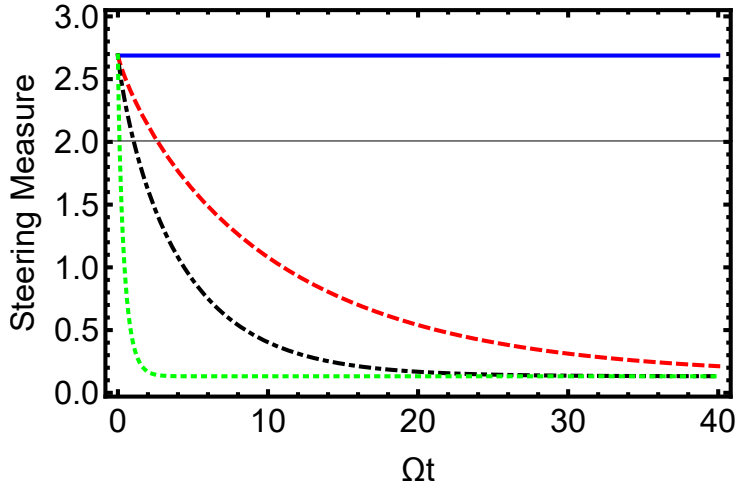

(**a**)

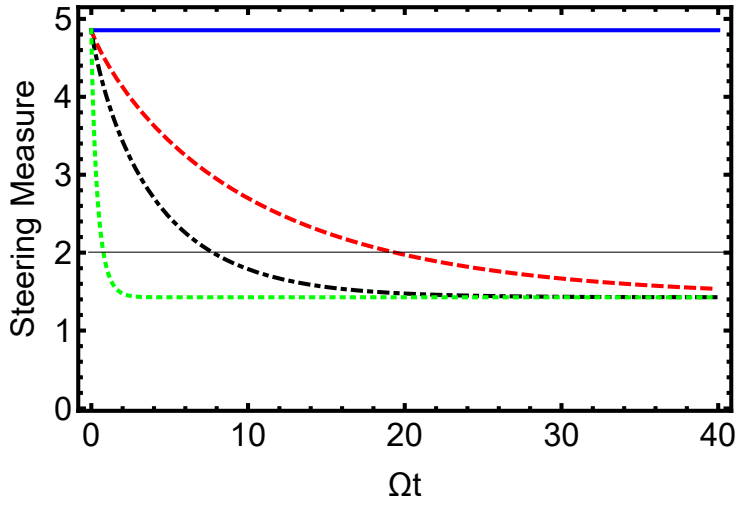

(**b**)

Figure 2. Time evolution of the quantum steering measure as a function of dimensionless time Ωt for initial conditions $b_1(0) = 1$, $b_2(0) = -0.6$, and $b_3(0) = 0.3$. Subfigures (**a**,**b**) depict the dynamics of quantum steering for different initial states: (**a**) $b_1(0) = 1$, $b_2(0) = -0.6$, $b_3(0) = 0.3$; and (**b**) $b_1(0) = 1$, $b_2(0) = -0.9$, $b_3(0) = 0.9$. The blue line represents $\kappa = 0$, the red dashed line corresponds to $\kappa = 0.02\ \Omega$, the black dash-dotted line indicates $\kappa = 0.05\ \Omega$, and the green dotted line denotes $\kappa = 0.5\ \Omega$, illustrating the effect of increasing decoherence on the quantum steering measure.

4.3. Analysis of Purity Dynamics Under Dephasing

Figure 3 demonstrates the evolution of quantum purity under various dephasing strengths, revealing fundamental aspects of coherence loss in the hydrogen hyperfine system. In subfigure (a), corresponding to initial state $[b_1(0) = 1, b_2(0) = -0.6, b_3(0) = 0.3]$, purity maintains constant unitary evolution ($\mathcal{P} \approx 0.6$) for $\kappa = 0$, while progressively faster decay to the maximally mixed state ($\mathcal{P} = 0.25$) occurs with increasing κ, reaching

complete mixing around $t \approx 2/\Omega$ for strong dephasing ($\kappa = 0.5\ \Omega$). Subfigure (b), representing the more strongly correlated initial state $[b_1(0) = 1, b_2(0) = -0.9, b_3(0) = 0.9]$, exhibits identical steady-state behavior but distinct transient dynamics, with initial purity values near $\mathcal{P} \approx 0.9$ reflecting the state's higher initial coherence, though all trajectories ultimately converge to the $\mathcal{P} \approx 0.45$ completely mixed state regardless of initial conditions, highlighting purity's role as a global measure of environmental decoherence that depends on decoherence strength rather than specific correlation patterns.

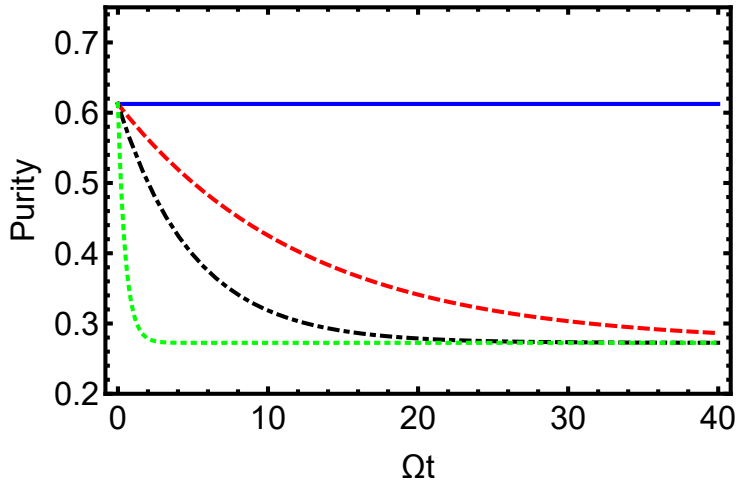

(**a**)

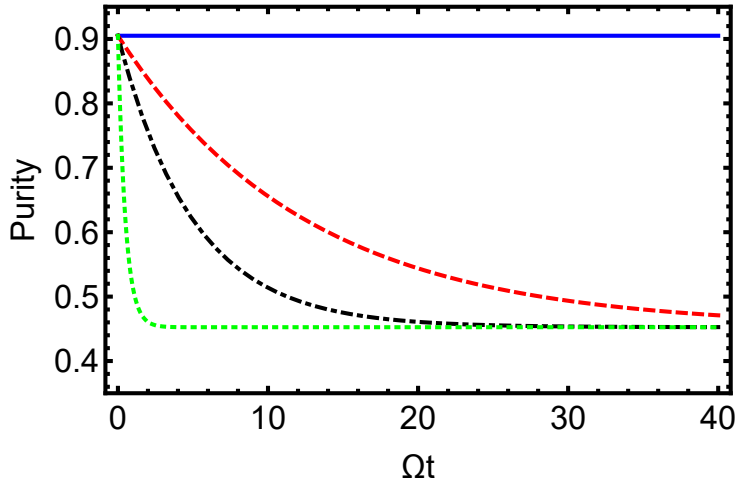

(**b**)

Figure 3. Time evolution of the purity as a function of dimensionless time Ωt for initial conditions $b_1(0) = 1$, $b_2(0) = -0.6$, and $b_3(0) = 0.3$. Subfigures (**a**,**b**) depict the dynamics of state purity for different initial states: (**a**) $b_1(0) = 1$, $b_2(0) = -0.6$, $b_3(0) = 0.3$; and (**b**) $b_1(0) = 1$, $b_2(0) = -0.9$, $b_3(0) = 0.9$. The blue line represents $\kappa = 0$, the red dashed line corresponds to $\kappa = 0.02\ \Omega$, the black dash-dotted line indicates $\kappa = 0.05\ \Omega$, and the green dotted line denotes $\kappa = 0.5\ \Omega$, illustrating the effect of increasing decoherence on the purity.

4.4. Analysis of Werner-State Nonlocality Under Dephasing

Figure 4 reveals the monotonic decay of Bell nonlocality under environmental decoherence for Werner states in 3d-plot. In subfigure (a), weak dephasing ($\kappa = 0.02\ \Omega$) results in a gradual decay of nonlocality, where states with higher initial purity (larger a values) maintain nonlocal characteristics for extended durations. The smooth decay profile indicates a memoryless Markovian process where coherence is steadily eroded without revivals. In contrast, subfigure (b) under strong dephasing ($\kappa = 0.5\ \Omega$) demonstrates rapid,

immediate suppression of nonlocality across all initial states. The near-vertical decay front shows that environmental noise dominates the dynamics, overwhelming the hyperfine interaction and driving the system to local behavior on timescales much shorter than the natural coherent evolution period. The absence of oscillatory behavior in both regimes confirms that dephasing effectively suppresses the coherent exchange of quantum correlations between the electron and proton spins, leading to irreversible loss of nonlocality.

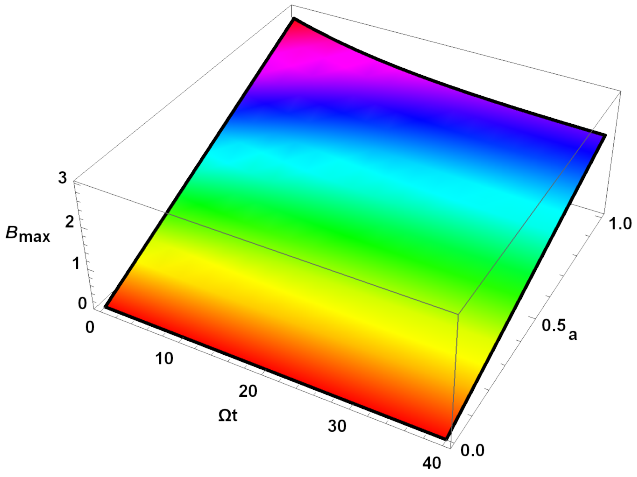

(**a**)

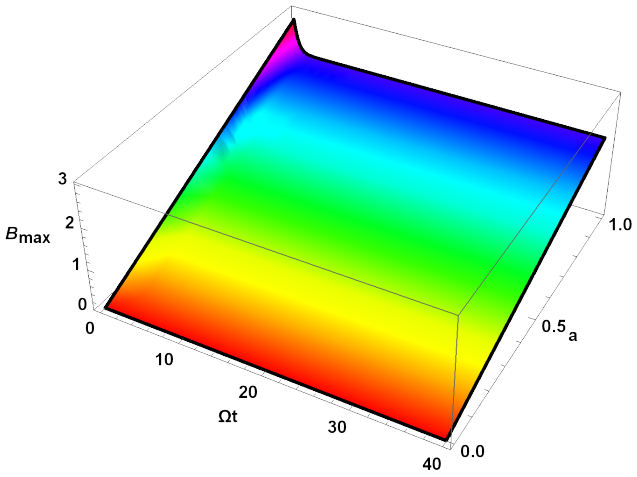

(**b**)

Figure 4. Time evolution of Bell nonlocality as a function of dimensionless time Ωt and the initial Werner state with parameter a. The subfigures (**a**,**b**) illustrate the time evolution of the Bell nonlocality under varying dephasing parameter κ, corresponding to $\kappa = 0.02\ \Omega$ and $\kappa = 0.5\ \Omega$, respectively.

Figure 5 demonstrates the degradation of quantum steering for Werner states under different dephasing strengths. In subfigure (a), weak dephasing ($\kappa = 0.02\ \Omega$) allows steering to persist for considerable durations, particularly for states with high initial purity ($a \to 1$). The gradual decay profile shows a smooth transition from steerable to non-steerable states, with the steering measure maintaining nonzero values across a broad parameter range before eventual extinction. Subfigure (b) under strong dephasing ($\kappa = 0.5\ \Omega$) reveals rapid destruction of steering capabilities, where even highly pure initial states lose their steerable character almost immediately. The sharp decay front indicates that strong environmental noise quickly overwhelms the quantum correlations necessary for steering, reducing the survival time of steerable states to a small fraction of the coherent evolution timescale. Comparison with Bell nonlocality dynamics reveals that steering exhibits intermediate

robustness, surviving longer than nonlocality but ultimately succumbing to environmental decoherence in a similar monotonic fashion, confirming the hierarchical relationship between these quantum correlation measures in open quantum systems.

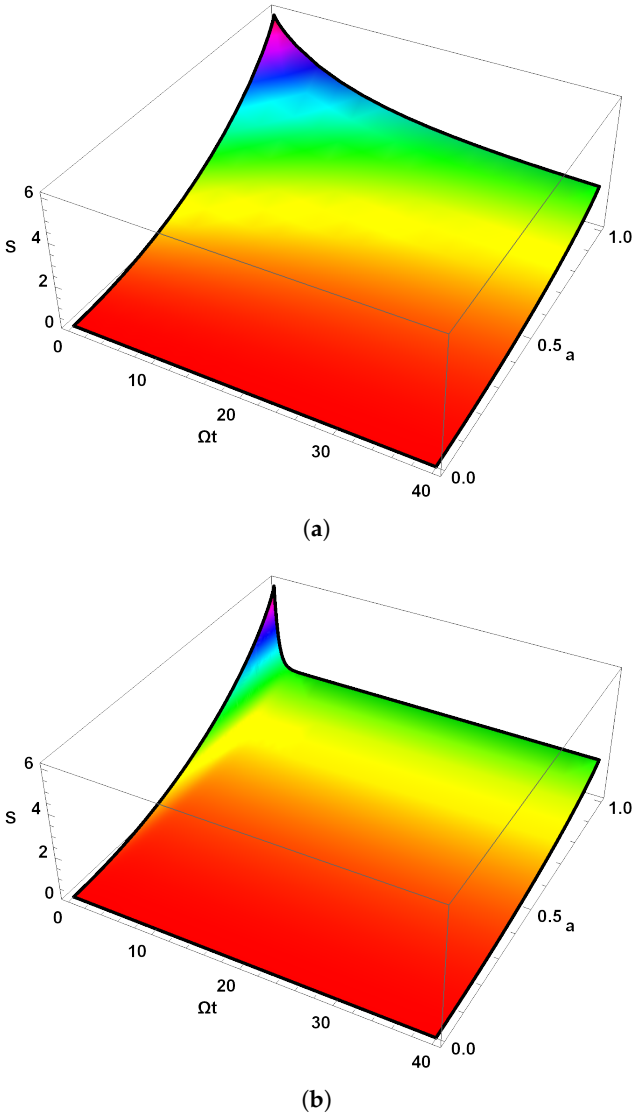

Figure 5. Time evolution of steering measure as a function of dimensionless time Ωt and the initial Werner state with parameter a. The subfigures (**a**,**b**) illustrate the time evolution of the quantum steering under varying dephasing parameter κ, corresponding to $\kappa = 0.02\ \Omega$ and $\kappa = 0.5\ \Omega$, respectively.

Figure 6 illustrates the universal degradation of quantum purity for Werner states under dephasing environments. In subfigure (a), weak dephasing ($\kappa = 0.02\ \Omega$) induces a gradual decay of purity across all initial states, with the rate of decoherence showing minimal dependence on the initial Werner parameter a. All trajectories converge toward the maximally mixed state ($\mathcal{P} = 0.25$) for large relative time, demonstrating that even modest environmental interaction eventually erases all quantum coherence. Subfigure (b) under strong dephasing ($\kappa = 0.5\ \Omega$) exhibits dramatically accelerated purity loss, where complete mixing occurs within relatively large time, representing a five-fold increase in decoherence rate compared to the weak damping case. The rapid collapse to the completely mixed state highlights the dominant role of environmental noise over the initial state preparation. Notably, unlike Bell nonlocality and steering which display hierarchical decay patterns dependent on initial correlations, purity evolution shows universal behavior across all

Werner states for a given dephasing strength, confirming its role as a global measure of environmental decoherence that is insensitive to the specific nature of quantum correlations.

The critical purity thresholds identified in the three-dimensional analysis mark the boundary below which Bell nonlocality is completely destroyed by dephasing noise. Physically, these thresholds quantify the extreme fragility of Bell nonlocality—the strongest form of quantum correlation—to loss of coherence, making it the first resource to disappear in realistic open-system conditions. In experimental contexts involving hyperfine spins, achieving and maintaining purity above the critical level requires exceptionally low dephasing rates, high-fidelity state preparation, and effective dynamical decoupling or error-mitigation techniques. Consequently, the thresholds provide a clear quantitative guideline for the maximum tolerable environmental noise and minimum required coherence times if Bell inequality violation is to be observed or exploited for device-independent quantum protocols. States that start very close to maximal purity can tolerate significantly more decoherence before losing nonlocality than states prepared with moderate initial purity, emphasizing the crucial importance of near-perfect initial Bell-state generation in noisy environments.

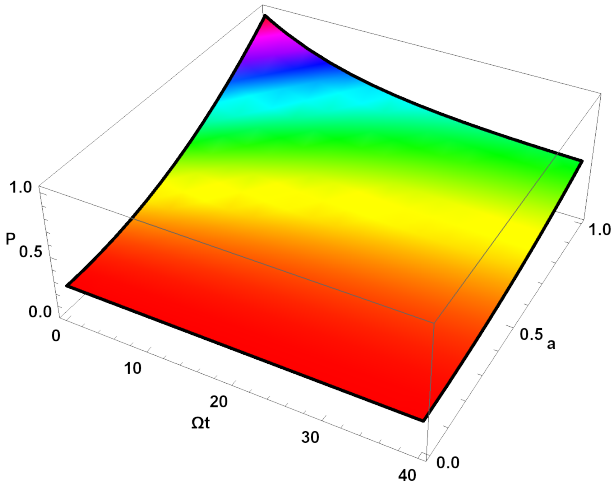

(**a**)

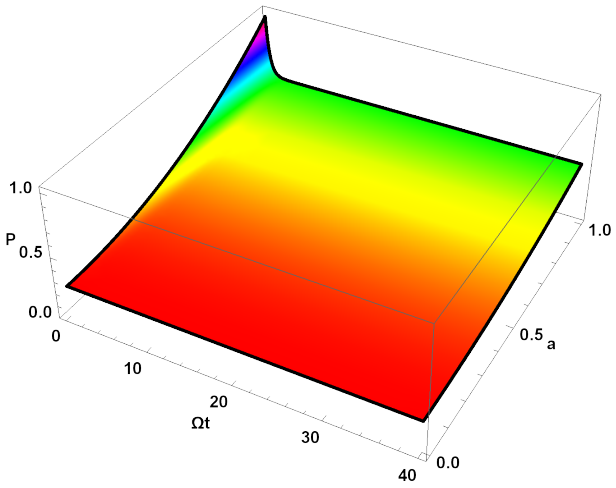

(**b**)

Figure 6. Time evolution of purity as a function of dimensionless time Ωt and the initial Werner state with parameter a. The subfigures (**a**,**b**) illustrate the time evolution of the purity state under varying dephasing parameter κ, corresponding to $\kappa = 0.02\,\Omega$ and $\kappa = 0.5\,\Omega$, respectively.

5. Conclusions

In this work, we have analyzed the interplay between magnetic coupling, quantum correlations, and environmental dephasing in atomic hydrogen. We examined the 1 s hyperfine state to identify the spin coupling that generated entangled states. By incorporating phase decoherence, we characterized how these correlations degraded over time and how initial entanglement affected nonclassical behavior. We quantified correlations using Bell nonlocality, EPR steering, and purity, each addressing a distinct level in the quantum hierarchy. Bell nonlocality tested violations of local realism, EPR steering explored asymmetric remote influence, and purity measured state mixedness linked to decoherence. Numerical simulations showed that without dephasing, all measures remained constant, confirming coherence stability. With increasing dephasing, each decayed exponentially to a lower bound, indicating quantum loss. Bell nonlocality proved most fragile, vanishing first, followed by steering and purity, aligning with correlation hierarchy. A three-dimensional Werner-state analysis revealed purity thresholds for Bell violations, linking mixedness and nonlocality. Overall, the study illustrated how magnetic coupling, decoherence, and initial entanglement shaped correlation persistence in open systems. It emphasized Bell nonlocality's sensitivity to noise and the relative resilience of steering and purity. These insights informed quantum information processing, highlighting the need to address hierarchical fragility in spin systems. Techniques like dynamical decoupling and state engineering could extend nonclassical resource lifetimes in practical settings. Finally, the predicted fragility hierarchy and critical purity thresholds are within reach of current experiments. EPR steering and Bell inequality violations in hyperfine spin systems have already been observed in analogous platforms such as trapped 87Rb atoms, ensembles of cold alkali atoms, and nitrogen-vacancy centers in diamond, using microwave/RF manipulation and high-fidelity projective measurements or state tomography. Controlled dephasing can be introduced via engineered magnetic-field noise or collisional effects, while dynamical decoupling sequences can extend coherence times sufficiently to probe the distinct decay rates of nonlocality, steering, and purity reported here, thereby offering direct experimental verification of our results in the near future.

Author Contributions: K.B. and S.B.: Writing—review and editing, Methodology, Investigation, Formal analysis, Conceptualization. All authors have read and agreed to the published version of the manuscript.

Funding: This work was supported and funded by the Deanship of Scientific Research at Imam Mohammad Ibn Saud Islamic University (IMSIU) (grant number IMSIU-DDRSP2503).

Data Availability Statement: The original contributions presented in this study are included in the article. Further inquiries can be directed to the corresponding author.

Conflicts of Interest: The authors declare that they have no known competing financial interests or personal relationships that could have appeared to influence the work reported in this paper.

Appendix A. Detailed Derivation of the Exact Time-Dependent Density Matrix Under Dephasing

The derivation starts from the system of differential Equations (11)–(20) obtained from the Lindblad master equation with local τ^z-dephasing channels (κ_e for the electron spin and κ_N for the proton spin) and uses the general X-state initial condition (21).

The initial density operator is the general two-qubit X-state

$$\varrho(0) = \frac{1}{4}\begin{pmatrix} 1+b_3 & 0 & 0 & b_1-b_2 \\ 0 & 1-b_3 & b_1+b_2 & 0 \\ 0 & b_1+b_2 & 1-b_3 & 0 \\ b_1-b_2 & 0 & 0 & 1+b_3 \end{pmatrix}, \tag{A1}$$

with real parameters $b_1, b_2, b_3 \in [-1, 1]$. The computational basis is $|1\rangle = |\uparrow_e\uparrow_N\rangle$, $|2\rangle = |\uparrow_e\downarrow_N\rangle$, $|3\rangle = |\downarrow_e\uparrow_N\rangle$, $|4\rangle = |\downarrow_e\downarrow_N\rangle$.

Equations (11) and (14) immediately yield

$$\frac{d\varrho_{11}}{dt} = 0, \qquad \frac{d\varrho_{44}}{dt} = 0 \quad \Longrightarrow \quad \varrho_{11}(t) = \varrho_{44}(t) = \frac{1+b_3}{4}. \tag{A2}$$

Equations (12)–(13) are

$$\frac{d\varrho_{22}}{dt} = -2i\Omega(\varrho_{23} - \varrho_{32}), \qquad \frac{d\varrho_{33}}{dt} = +2i\Omega(\varrho_{23} - \varrho_{32}). \tag{A3}$$

Define $\delta(t) \equiv \varrho_{22}(t) - \varrho_{33}(t)$. Then, $\frac{d\delta}{dt} = -4i\Omega(\varrho_{23} - \varrho_{32})$. As shown below, $\varrho_{23}(t)$ remains real for all t, so $\varrho_{23} - \varrho_{32} = 0$ and $\frac{d\delta}{dt} = 0$. Because $\delta(0) = 0$, we have $\delta(t) = 0\ \forall t$, i.e.,

$$\varrho_{22}(t) = \varrho_{33}(t) = \frac{1-b_3}{4}. \tag{A4}$$

Equation (17) is already decoupled:

$$\frac{d\varrho_{14}}{dt} = -2(\kappa_e + \kappa_N)\varrho_{14}. \tag{A5}$$

Integrating with the initial value $\varrho_{14}(0) = (b_1 - b_2)/4$ gives

$$\varrho_{14}(t) = \frac{b_1 - b_2}{4}\, e^{-2(\kappa_e+\kappa_N)t}. \tag{A6}$$

Equation (18), derived from the commutator $[H_M, \varrho]$ and the dephasing dissipator, reads

$$\frac{d\varrho_{23}}{dt} = 2i\Omega(\varrho_{22} - \varrho_{33}) - 2(\kappa_e + \kappa_N)\varrho_{23}. \tag{A7}$$

The term $(\varrho_{22} - \varrho_{33})$ vanishes identically, yielding

$$\frac{d\varrho_{23}}{dt} = -2(\kappa_e + \kappa_N)\varrho_{23}. \tag{A8}$$

The solution with initial value $\varrho_{23}(0) = (b_1 + b_2)/4$ is

$$\varrho_{23}(t) = \frac{b_1 + b_2}{4}\, e^{-2(\kappa_e+\kappa_N)t}. \tag{A9}$$

The right-hand side is real and the initial condition is real, so $\varrho_{23}(t)$ remains real at all times.

The remaining off-diagonal elements satisfy two decoupled systems:

$$\dot{\varrho}_{12} = -2i\Omega(\varrho_{12} - \varrho_{13}) - 2\kappa_N\varrho_{12}, \tag{A10}$$

$$\dot{\varrho}_{13} = -2i\Omega(\varrho_{13} - \varrho_{12}) - 2\kappa_e\varrho_{13}, \tag{A11}$$

and

$$\dot{\varrho}_{24} = -2i\Omega(\varrho_{24} - \varrho_{34}) - 2\kappa_e\varrho_{24}, \tag{A12}$$

$$\dot{\varrho}_{34} = -2i\Omega(\varrho_{34} - \varrho_{24}) - 2\kappa_N\varrho_{34}. \tag{A13}$$

In vector form $\mathbf{v}(t) = \begin{pmatrix} \varrho_{12}(t) \\ \varrho_{13}(t) \end{pmatrix}$, we have

$$\dot{\mathbf{v}}(t) = \mathcal{L}_1\mathbf{v}(t), \qquad \mathcal{L}_1 = \begin{pmatrix} -2i\Omega - 2\kappa_N & 2i\Omega \\ 2i\Omega & 2i\Omega - 2\kappa_e \end{pmatrix}. \tag{A14}$$

This is a linear system with constant coefficients. The general solution is

$$\mathbf{v}(t) = e^{\mathcal{L}_1 t}\mathbf{v}(0). \tag{A15}$$

For the X-state initial condition (21), $\varrho_{12}(0) = \varrho_{13}(0) = 0$, so $\mathbf{v}(0) = \mathbf{0}$. Therefore,

$$\varrho_{12}(t) = \varrho_{13}(t) \equiv 0 \quad \forall t \geq 0. \tag{A16}$$

In vector form $\mathbf{w}(t) = \begin{pmatrix} \varrho_{24}(t) \\ \varrho_{34}(t) \end{pmatrix}$, we have

$$\dot{\mathbf{w}}(t) = \mathcal{L}_2\mathbf{w}(t), \qquad \mathcal{L}_2 = \begin{pmatrix} -2i\Omega - 2\kappa_e & 2i\Omega \\ 2i\Omega & 2i\Omega - 2\kappa_N \end{pmatrix}. \tag{A17}$$

Again, the X-state initial condition gives $\varrho_{24}(0) = \varrho_{34}(0) = 0$, so $\mathbf{w}(0) = \mathbf{0}$. Hence,

$$\varrho_{24}(t) = \varrho_{34}(t) \equiv 0 \quad \forall t \geq 0. \tag{A18}$$

Defining $\kappa \equiv \kappa_e + \kappa_N$, the exact solution preserving the X-structure for all times is

$$\varrho(t) = \begin{pmatrix} \frac{1+b_3}{4} & 0 & 0 & \frac{b_1-b_2}{4}e^{-2\kappa t} \\ 0 & \frac{1-b_3}{4} & \frac{b_1+b_2}{4}e^{-2\kappa t} & 0 \\ 0 & \frac{b_1+b_2}{4}e^{-2\kappa t} & \frac{1-b_3}{4} & 0 \\ \frac{b_1-b_2}{4}e^{-2\kappa t} & 0 & 0 & \frac{1+b_3}{4} \end{pmatrix}. \tag{A19}$$

This closed-form expression is used throughout the paper to evaluate the time evolution of Bell nonlocality, EPR steering, and quantum purity.

References

1. Einstein, A.; Podolsky, B.; Rosen, N. Can Quantum-Mechanical Description of Physical Reality Be Considered Complete? *Phys. Rev.* **1935**, *47*, 777–780. [CrossRef]
2. Nilsen, M.A.; Chuang, I.L. *Quantum Computation and Quantum Communication*; Cambridge University Press: Cambridge, UK, 2000.
3. Horodecki, R.; Horodecki, P.; Horodecki, M.; Horodecki, K. Quantum entanglement. *Rev. Mod. Phys.* **2009**, *81*, 865. [CrossRef]
4. Bennett, C.H.; DiVincenzo, D.P. Quantum information and computation. *Nature* **2000**, *404*, 247–255. [CrossRef]
5. Berrada, K.; Eleuch, H. Noncommutative deformed cat states under decoherence. *Phys. Rev. D* **2019**, *100*, 016020. [CrossRef]
6. Berrada, K. Quantum metrology with SU(1,1) coherent states in the presence of nonlinear phase shifts. *Phys. Rev. A* **2013**, *88*, 013817. [CrossRef]
7. Zheng, S.B.; Guo, G.C. Efficient Scheme for Two-Atom Entanglement and Quantum Information Processing in Cavity QED. *Phys. Rev. Lett.* **2000**, *85*, 2392. [CrossRef]

8. Castelano, L.K.; Fanchini, F.F.; Berrada, K. Open quantum system description of singlet-triplet qubits in quantum dots. *Phys. Rev B* **2016**, *94*, 235433. [CrossRef]
9. Bell, J.S. On the Einstein Podolsky Rosen paradox. *Physics* **1964**, *1*, 195.
10. Schrödinger, E. Probability relations between separated systems. *Math. Proc. Camb. Phil. Soc.* **1936**, *32*, 446. [CrossRef]
11. Wiseman, H.M.; Jones, S.J.; Doherty, A.C. Steering, Entanglement, Nonlocality, and the Einstein-Podolsky-Rosen Paradox. *Phys. Rev. Lett.* **2007**, *98*, 140402. [CrossRef]
12. Saunders, D.J.; Jones, S.J.; Wiseman, H.M.; Pryde, G.J. Experimental EPR-steering using Bell-local states. *Nat. Phys.* **2010**, *6*, 845. [CrossRef]
13. Wollmann, S.; Walk, N.; Bennet, A.J.; Wiseman, H.M.; Pryde, G.J. Observation of Genuine One-Way Einstein-Podolsky-Rosen Steering. *Phys. Rev. Lett.* **2016**, *116*, 160403. [CrossRef]
14. Gehring, T.; Händchen, V.; Duhme, J.; Furrer, F.; Franz, T.; Pacher, C.; Werner, R.F.; Schnabel, R. Implementation of Continuous-Variable Quantum Key Distribution with Composable and One-Sided-Device-Independent Security Against Coherent Attacks. *Nat. Commun.* **2015**, *6*, 8795. [CrossRef]
15. Cavalcanti, E.G.; Jones, S.J.; Wiseman, H.M.; Reid, M.D. Experimental criteria for steering and the Einstein-Podolsky-Rosen paradox. *Phys. Rev. A* **2009**, *80*, 032112. [CrossRef]
16. Wittmann, B.; Ramelow, S.; Steinlechner, F.; Langford, N.K.; Brunner, N.; Wiseman, H.M.; Ursin, R.; Zeilinger, A. Loophole-free Einstein-Podolsky-Rosen experiment via quantum steering. *New J. Phys.* **2012**, *14*, 053030. [CrossRef]
17. Piani, M.; Watrous, J. Necessary and Sufficient Quantum Information Characterization of Einstein-Podolsky-Rosen Steering. *Phys. Rev. Lett.* **2015**, *114*, 060404. [CrossRef] [PubMed]
18. Branciard, C.; Cavalcanti, E.G.; Walborn, S.P.; Scarani, V.; Wiseman, H.M. One-sided device-independent quantum key distribution: Security, feasibility, and the connection with steering. *Phys. Rev. A* **2012**, *85*, 010301. [CrossRef]
19. He, Q.; Rosales-Zárate, L.; Adesso, G.; Reid, M.D. Secure Continuous Variable Teleportation and Einstein-Podolsky-Rosen Steering. *Phys. Rev. Lett.* **2015**, *115*, 180502. [CrossRef]
20. Jones, S.J.; Wiseman, H.M.; Doherty, A.C. Entanglement, Einstein-Podolsky-Rosen correlations, Bell nonlocality, and steering. *Phys. Rev. A* **2007**, *76*, 052116. [CrossRef]
21. Skrzypczyk, P.; Navascués, M.; Cavalcanti, D. Quantifying Einstein-Podolsky-Rosen Steering. *Phys. Rev. Lett.* **2014**, *112*, 180404. [CrossRef]
22. Walborn, S.P.; Salles, A.; Gomes, R.M.; Toscano, F.; Ribeiro, P.H.S. Revealing Hidden Einstein-Podolsky-Rosen Nonlocality. *Phys. Rev. Lett.* **2011**, *106*, 130402. [CrossRef]
23. Zhen, Y.; Zheng, Y.; Cao, W.; Li, L.; Chen, Z.; Liu, N.; Chen, K. Certifying Einstein-Podolsky-Rosen steering via the local uncertainty principle. *Phys. Rev. A* **2016**, *93*, 012108. [CrossRef]
24. Zukowski, M.; Dutta, A.; Yin, Z. Geometric Bell-like inequalities for steering. *Phys. Rev. A* **2015**, *91*, 032107. [CrossRef]
25. Girdhar, P.; Cavalcanti, E.G. All two-qubit states that are steerable via Clauser-Horne-Shimony-Holt-type correlations are Bell nonlocal. *Phys. Rev. A* **2016**, *94*, 032317. [CrossRef]
26. Bohr, N. On the constitution of atoms and molecules. *Philos. Mag.* **1913**, *26*, 1. [CrossRef]
27. Bethe, H.; Salpeter, E. *Quantum Mechanics of One- and Two-Electron Atoms*; Springer: Berlin/Heidelberg, Germany, 1957.
28. Series, G.W. *Spectrum of Atomic Hydrogen*; Oxford University: New York, NY, USA, 1957.
29. Landau, L.D.; Lifshitz, E.M. *Quantum Mechanics: The Basic Concepts*, 3rd ed.; Elsevier: Oxford, UK, 1977. [CrossRef]
30. Sheludiakov, S.; McColgan, P.T.; Lee, D.M.; Khmelenko, V.V.; Järvinen, J.; Ahokas, J.; Vasiliev, S. Formation of Nuclear-Polarized Phases of H Atoms Embedded in Solid H2 Films. *Phys. Rev. Lett.* **2019**, *122*, 225301. [CrossRef] [PubMed]
31. Ahokas, J.; Vainio, O.; Novotny, S.; Järvinen, J.; Khmelenko, V.V.; Lee, D.M.; Vasiliev, S. Magnetic resonance study of H atoms in thin films of H2 at temperatures below 1 K. *Phys. Rev. B* **2010**, *81*, 104516. [CrossRef]
32. Ahokas, J.; Järvinen, J.; Khmelenko, V.V.; Lee, D.M.; Vasiliev, S. Exotic Behavior of Hydrogen Atoms in Solid H2 at Temperatures below 1 K. *Rev. Lett.* **2006**, *97*, 095301. [CrossRef] [PubMed]
33. Bigelow, N.P.; Freed, J.H.; Lee, D.M. Nuclear-spin waves in polarized atomic hydrogen gas: Temperature and density dependence in the hydrodynamic and Knudsen regimes. *Phys. Rev. Lett.* **1989**, *63*, 1609. [CrossRef]
34. Johnson, A.C.; Petta, J.R.; Taylor, J.M.; Yacoby, A.; Lukin, M.D.; Marcus, C.M.; Hanson, M.P.; Gossard, A.C. Triplet–singlet spin relaxation via nuclei in a double quantum dot. *Nature* **2005**, *435*, 925. [CrossRef]
35. Petta, J.R.; Johnson, A.C.; Taylor, J.M.; Laird, E.A.; Yacoby, A.; Lukin, M.D.; Marcus, C.M.; Hanson, M.P.; Gossard, A.C. Coherent Manipulation of Coupled Electron Spins in Semiconductor Quantum Dots. *Science* **2005**, *309*, 2180. [CrossRef] [PubMed]
36. Taylor, J.M.; Engel, H.A.; Dür, W.; Yacoby, A.; Marcus, C.M.; Zoller, P.; Lukin, M.D. Fault-tolerant architecture for quantum computation using electrically controlled semiconductor spins. *Nat. Phys.* **2005**, *1*, 177. [CrossRef]
37. Ladd, T.D.; Jelezko, F.; Laflamme, R.; Nakamura, Y.; Monroe, C.; O'Brien, J.L. Quantum Computing. *Nature* **2010**, *464*, 45. [CrossRef]
38. Childress, L.; Gurudev Dutt, M.V.; Taylor, J.M.; Zibrov, A.S.; Jelezko, F.; Wrachtrup, J.; Hemmer, P.R.; Lukin, M.D. Coherent Dynamics of Coupled Electron and Nuclear Spin Qubits in Diamond. *Science* **2006**, *314*, 281. [CrossRef]

39. Dutt, M.G.; Childress, L.; Jiang, L.; Togan, E.; Maze, J.; Jelezko, F.; Zibrov, A.S.; Hemmer, P.R.; Lukin, M.D.Quantum Register Based on Individual Electronic and Nuclear Spin Qubits in Diamond. *Science* **2007**, *316*, 1312. [CrossRef]
40. Neumann, P.; Mizuochi, N.; Rempp, F.; Hemmer, P.; Watanabe, H.; Yamasaki, S.; Jacques, V.; Gaebel, T.; Jelezko, F.; Wrachtrup, J. Multipartite Entanglement Among Single Spins in Diamond. *Science* **2008**, *320*, 1326. [CrossRef]
41. Fuchs, G.D.; Dobrovitski, V.V.; Toyli, D.M.; Heremans, F.J.; Awschalom, D.D. Gigahertz Dynamics of a Strongly Driven Single Quantum Spin. *Science* **2009**, *326*, 1520. [CrossRef]
42. Tommassini, P.; Timmermans, E.; Piza, A.F.R.d. The hydrogen atom as an entangled electron–proton system. *Am. J. Phys.* **1998**, *66*, 881. [CrossRef]
43. Zhu, G.-Q.; Du, K.-C.; Li, Y.-Q. Electron-nuclear entanglement in hydrogen atom. *Phys. A* **2005**, *346*, 295. [CrossRef]
44. Lindblad, G. On the generators of quantum dynamical semigroups. *Commun. Math. Phys.* **1976**, *48*, 119. [CrossRef]
45. Breuer, H.-P.; Petruccione, F. *The Theory of Open Quantum Systems*; Oxford University Press: Oxford, UK, 2002.
46. Berrada, K.; Bougouffa, S. Quantum Coherence and Mixedness in Hydrogen Atoms: Probing Hyperfine Structure Dynamics Under Dephasing Constraints. *Symmetry* **2025**, *17*, 1633 [CrossRef]
47. Berrada, K.; Bougouffa, S. Harnessing Quantum Entanglement and Fidelity in Hydrogen Atoms: Unveiling Dynamics Under Dephasing Noise. *Appl. Sci.* **2025**, *15*, 10938. [CrossRef]
48. Crawford, S.E.; Shugayev, R.A.; Paudel, H.P.; Lu, P.; Syamlal, M.; Ohodnicki, P.R.; Chorpening, B.; Gentry, R.; Duan, Y. Quantum Sensing for Energy Applications: Review and Perspective. *Adv. Quantum Technol.* **2021**, *4*, 2100049. [CrossRef]
49. Berrada, K.; Bougouffa, S. Quantum Coherence and Purity in Dissipative Hydrogen Atoms: Insights from the Lindblad Master Equation. *Entropy* **2025**, *27*, 848. [CrossRef] [PubMed]
50. Maleki, Y.; Sheludiakov, S.; Khmelenko, V.V.; Scully, M.O.; Lee, D.M.; Zheltikov, A.M. Natural and magnetically induced entanglement of hyperfine-structure states in atomic hydrogen. *Phys. Rev. A* **2021**, *103*, 052804. [CrossRef]
51. Abo, S.; Soubusta, J.; Jiráková, K.; Bartkiewicz, K.; Černoch, A.; Lemr, K.; Miranowicz, A. Experimental hierarchy of two-qubit quantum correlations without state tomography. *Sci. Rep.* **2023**, *13*, 8564. [CrossRef]
52. Ali, M. Effect of Classical and Quantum Superposition of Atomic States on Quantum Correlations. *Adv. High Energy Phys.* **2023**, *2023*, 2729561.
53. Demtröder, W. *Atoms, Molecules and Photons*; Springer: Berlin/Heidelberg, Germany, 2010.
54. Pethick, C.J.; Smith, H. *Bose–Einstein Condensation in Dilute Gases*; Cambridge University Press: Cambridge, UK, 2008.
55. Nathan, F.; Rudner, M.S. Universal Lindblad equation for open quantum systems. *Phys. Rev. B* **2020**, *102*, 115109. [CrossRef]
56. Manzano, D. A short introduction to the Lindblad master equation. *AIP Adv.* **2020**, *10*, 025106. [CrossRef]
57. Budini, A.A. Lindblad rate equations. *Phys. Rev. A* **2006**, *74*, 053815. [CrossRef]
58. Bennett, C.H.; Wiesner, S.J. Communication via one- and two-particle operators on Einstein-Podolsky-Rosen states. *Phys. Rev. Lett.* **1992**, *69*, 2881. [CrossRef] [PubMed]
59. Bouwmeester, D.; Pan, J.-W.; Mattle, K.; Eibl, M.; Weinfurter, H.; Zeilinger, A. Experimental quantum teleportation. *Nature* **1997**, *390*, 575. [CrossRef]
60. Furusawa, A.; Sørensen, J.L.; Braunstein, S.L.; Fuchs, C.A.; Kimble, H.J.; Polzik, E.S. Unconditional quantum teleportation. *Science* **1998**, *282*, 706. [CrossRef] [PubMed]
61. Clauser, J.F.; Horne, M.A.; Shimony, A.; Holt, R.A. Proposed experiment to test local hidden-variable theories. *Phys. Rev. Lett.* **1969**, *23*, 880. [CrossRef]
62. Aspect, A.; Grangier, P.; Roger, G. Experimental realization of Einstein-Podolsky-Rosen-Bohm Gedankenexperiment: A new violation of Bell's inequalities. *Phys. Rev. Lett.* **1982**, *49*, 91. [CrossRef]
63. Brunner, N.; Cavalcanti, D.; Pironio, S.; Scarani, V.; Wehner, S. Bell nonlocality. *Rev. Mod. Phys.* **2014**, *86*, 419. [CrossRef]
64. Gisin, N. Bell's inequality holds for all non-product states. *Phys. Lett. A* **1991**, *154*, 201. [CrossRef]
65. Nielsen, M.A.; Chuang, I.L. *Quantum Computation and Quantum Information*; Cambridge University Press: Cambridge, UK, 2010.
66. Bengtsson, I.; Życzkowski, K. *Geometry of Quantum States: An Introduction to Quantum Entanglement*, 2nd ed.; Cambridge University Press: Cambridge, UK, 2017.
67. Wilde, M.M. *Quantum Information Theory*, 2nd ed.; Cambridge University Press: Cambridge, UK, 2017.
68. van Meter, J.R. Quantum Coherence in Atomic Hydrogen: Probing 21 cm Hyperfine Transitions. *Phys. Rev. A* **2006**, *74*, 063804.
69. Preskill, J. *Lecture Notes on Quantum Computation*; California Institute of Technology: Pasadena, CA, USA, 1998.